foods

MDPI

Article

Numerical Study on the Variable-Temperature Drying and Rehydration of Shiitake

Lizhe Zhang, Long Jiang, Meriem Adnouni, Sheng Li and Xuejun Zhang *

Key Laboratory of Refrigeration and Cryogenic Technology of Zhejiang Province, Institute of Refrigeration and Cryogenics, Zhejiang University, Hangzhou 310027, China; zhanglizhe@zju.edu.cn (L.Z.)
* Correspondence: xuejzhang@zju.edu.cn

Abstract: Variable-temperature convective drying (VTCD) is a promising technology for obtaining high-quality dried mushrooms, particularly when considering rehydration capacity. However, accurate numerical models for variable-temperature convective drying and rehydration of shiitake mushrooms are lacking. This study addresses this gap by employing a model with thermo–hydro and mechanical bidirectional coupling to investigate five dehydration characteristics (moisture ratio, drying rate, temperature, evaporation rate, and volume shrinkage ratio) and a drying load characteristic (enthalpy difference) during VTCD. Additionally, a mathematical model combining drying and rehydration is proposed to analyze the effect of VTCD processes on the rehydration performance of shiitake mushrooms. The results demonstrate that, compared to constant-temperature drying, VTCD-dried mushrooms exhibit moderate shrinkage rates and drying time (16.89 h), along with reduced temperature variation and evaporation rate gradient (Max. 1.50 mol/(m^3·s)). VTCD also improves enthalpy stability, reducing the maximum drying load by 58.84% compared to 338.15 K constant-temperature drying. Furthermore, drying time at medium temperatures (318.15–328.15 K) greatly influences rehydration performance. This study quantitatively highlights the superiority of variable-temperature convective drying, offering valuable insights for optimizing the shiitake mushroom drying processes.

Keywords: shiitake mushroom; variable-temperature convective drying; drying characteristics; rehydration

check for updates

Citation: Zhang, L.; Jiang, L.; Adnouni, M.; Li, S.; Zhang, X. Numerical Study on the Variable-Temperature Drying and Rehydration of Shiitake. *Foods* **2024**, *13*, 3356. https://doi.org/10.3390/foods13213356

Academic Editors: Biljana Lončar and Lato Pezo

Received: 29 September 2024
Revised: 17 October 2024
Accepted: 18 October 2024
Published: 23 October 2024

Copyright: © 2024 by the authors. Licensee MDPI, Basel, Switzerland. This article is an open access article distributed under the terms and conditions of the Creative Commons Attribution (CC BY) license (https://creativecommons.org/licenses/by/4.0/).

1. Introduction

Shiitake mushroom is a popular type of macrofungi with high nutritional value and health-promoting properties. It is the second most cultivated edible mushroom worldwide, accounting for about 25% of global mushroom production [1]. China produced over 11.88 million tons of shiitake mushrooms in 2020 [2]. However, this abundance presents a challenge, as fresh shiitake mushrooms have a high wet-basis moisture content of 85% to 90% [3]. Browning, lipid oxidation, and microbial deterioration occur when water interacts with the macromolecules of shiitake mushrooms [4]. The high moisture content necessitates significant drying efforts for preservation and further processing. In addition, dried shiitake mushrooms have a unique aroma and are more nutritious than fresh ones [5,6]. Thus, it is crucial to dry them in good time to improve their shelf life and quality.

Various drying methods have been studied for shiitake mushroom processing, including sun, convective, vacuum, microwave, infrared, heat pump, and freeze drying [7,8]. These approaches use different energy sources and equipment. Convective drying remains the most common drying approach due to its simplicity and practical advantages [4]. Heated air comes into direct contact with shiitake mushrooms, transferring heat and moisture by convection. Shiitake mushrooms are highly heat-sensitive. The most significant factor for shiitake mushroom convective drying is drying temperature, and its impacts on dehydration characteristics have been thoroughly researched. For instance, the shiitake

mushrooms' biological activity and heat-sensitive components are greatly influenced by drying temperature [9,10]. However, in most existing studies, the drying temperature for shiitake mushrooms remains constant, i.e., constant-temperature convective drying (CTCD). Recent research has discovered that shiitake mushrooms undergo complex physical and chemical changes during convective drying, which include aroma synthesis of enzymatic reactions and conversion between precursors and volatiles [11]. Therefore, the variable drying temperature is conducive to reducing the loss of heat-sensitive nutrients.

Variable-temperature convective drying (VTCD) optimizes the dried food quality by adjusting the drying temperature based on the food's thermal characteristics [12]. It is an adaptive drying process that can achieve the multi-objective optimization of the quality of specific dried products [13]. Compared to some new drying technologies that require high costs, ordinary convective drying technology combined with a variable-temperature strategy is an efficient and cost-effective option [14]. Zhang et al. [15] found that VTCD not only effectively controlled browning in the freeze–thaw pretreatment of lotus root but also reduced the drying time and energy consumption of the process. Ayadi et al. [16] compared the spearmint drying curves of four CTCD processes with those of two VTCD processes, finding that the temperature-increasing VTCD was the best for drying time and operating cost. Recently, the performance of VTCD on shiitake mushrooms has also been investigated, and the results showed that VTCD was better than CTCD in terms of the shiitake mushroom rehydration ratio, heat pump COP, and drying time [17].

Optimizing VTCD processes is crucial for improving dried shiitake mushroom quality and system energy efficiency [17]. Existing studies mainly focus on drying parameters [16,18,19], neglecting the dynamic matching between energy supply and demand. The dynamic changes of heat load and moisture load in the drying process are particularly complicated because of the porosity and biological characteristics of shiitake mushrooms [4]. On the one hand, excessive energy supply not only accelerates nutrient loss [20], shrinkage [21], and hardening [22], but also results in energy waste. On the other hand, insufficient energy supply leads to insufficient dehydration and longer drying time [23]. Compared to CTCD, VTCD has more potential for achieving the dynamic matching between energy supply and demand by dividing a whole drying process into several sub-processes [24]. Energy demand is relatively steady in each sub-process. However, few studies have investigated the superiority of VTCD in supply–demand matching.

The optimization indices of VTCD processes are like those of CTCD processes. Dried mushrooms must be rehydrated before consumption. Rehydration represents the ability of dried mushrooms in solution to restore the properties of fresh ones [25]. The rehydration performance of dried food products is related to cell structural damage [26], composition change, and shrinkage during drying. Therefore, it is considered an essential quality attribute for dried shiitake mushrooms. García-Segovia et al. [27] performed shiitake mushroom CTCD at 50 °C. They compared the rehydration kinetics of shiitake mushrooms under different rehydration temperatures and pressures, discovering that the vacuum process had a faster rehydration velocity at lower temperatures than the atmospheric process. High rehydration temperature (80 °C) caused structural damage that prevented water absorption. Qiu et al. [28] investigated the water-holding capacity of rehydrated shiitake mushrooms in different CTCD conditions. Their study found significant changes in the rehydration ratio and water-holding capacity from 40 °C to 70 °C. This showed that drying temperature significantly affected the interior structure of rehydrated shiitake mushrooms. However, there is still a lack of research on the relationship between VTCD processes and shiitake mushroom rehydration kinetics.

In addition, current research focuses primarily on experimental investigations on shiitake mushroom VTCD [17,29]. It is time-consuming and expensive to study various VTCD processes due to the need for customized experiment systems. Moreover, the variations in material properties among mushrooms affect the analysis of the results. Numerical models can be utilized to investigate shiitake mushroom VTCD characteristics at a lower expense and in less time. However, accurate numerical models are still lacking for

shiitake mushroom VTCD since it is a complex problem involving multiphysics processes, i.e., heat transfer, mass transfer, fluid flow, and shrinkage.

To fill the above gaps, this study aims to develop a comprehensive numerical model for shiitake mushroom VTCD by considering heat transfer, mass transfer, fluid flow, shrinkage, and interaction between physical field parameters. The model offers a cost-effective and time-saving alternative to traditional experimental methods. It investigates moisture ratio (MR), drying rate, temperature, evaporation rate, and volume shrinkage ratio of shiitake mushrooms during CTCD and VTCD. Additionally, the air enthalpy differences between the inlet and outlet of a chamber during CTCD and VTCD are compared to reveal energy demand patterns. Then, the relationship between VTCD processes and rehydration kinetics is examined, and a mathematical model combining drying and rehydration is established to analyze the effect of VTCD processes on the rehydration performance of shiitake mushrooms. Finally, the VTCD processes are evaluated based on the simulated water absorption capacity ratio to the total drying time to obtain an optimal drying process.

2. Materials and Methods

2.1. Materials and Instruments

Fresh shiitake mushrooms (*Lentinula edodes*) were harvested in September 2023 from Jinzifeng Edible Fungi Professional Cooperative in Qingyuan County, Zhejiang Province, China. The harvested mushrooms were immediately transported to the laboratory for refrigeration. Shiitake mushrooms' diameter and height were 0.056 ± 0.004 m and 0.025 ± 0.002 m, respectively. The initial moisture content was 85.50 ± 2.66% (wet-basis). Samples of mushrooms were selected, with bright colors, fine and orderly gills, no abnormal external moisture, and no damage. Their stipes were trimmed, and their surfaces were cleaned up. A transparent acrylic ventilation chamber (Figure 1) was placed in a constant temperature and humidity oven (DHTH-100-0-P-SD). Its size was 0.12 m (length) × 0.12 m (height) × 0.2 m (width). The chamber bottom was equipped with a stepless speed regulating fan to control air velocity, and a small hole with a diameter of 0.015 m was on its side to place a hot wire anemometer. Hot air entered from the bottom and flowed out from the top. The shiitake mushrooms were in a wire mesh tray 0.1 m from the chamber bottom. The volume of shiitake mushrooms was measured using quartz sand (0.425–0.7 mm), a beaker, a funnel, and two graduated cylinders. During the drying and rehydration processes, the mass was measured using an electronic balance with an accuracy of 0.001 g. Distilled water, filter paper, and a thermostatic bath were used for rehydration. Furthermore, the initial dry basis mass of the mushrooms was determined using an electric drying oven.

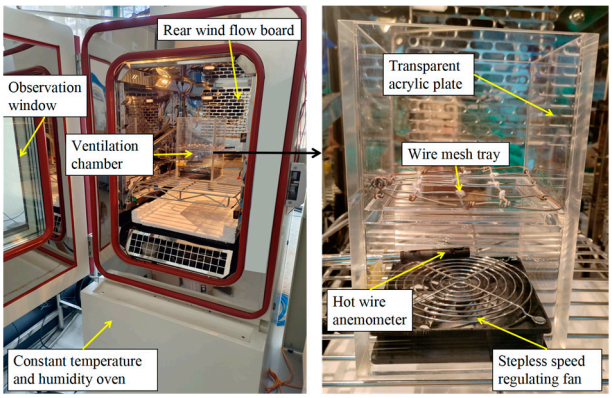


Figure 1. Experimental ventilation chamber.

2.2. Experimental Procedure

The shiitake mushroom drying experiments were conducted as follows: First, fresh mushrooms were removed from refrigeration and equilibrated to room temperature. Next, the ventilation chamber was preheated to a constant temperature and humidity to establish

the drying environment. Then, the initial mass and volume of the mushrooms were measured using an electronic balance and quartz sand [30]. Mushrooms were placed cap-side up on the tray, and their mass and volume were recorded at 30 min intervals during the first three hours, followed by hourly measurements. After drying, the initial moisture content was determined using the 105 °C oven method [17].

The dried mushrooms were first weighed for the rehydration experiments, and distilled water (thirty times the mushroom mass) was prepared [31,32]. Subsequently, the water was heated to 60 °C in a thermostatic bath, after which the dried mushrooms were immersed for five hours. Mass was measured every 30 min after removing excess surface water with filter paper. Lastly, both the rehydration liquid and rehydrated mushrooms were dried to constant weight at 105 °C to determine their dry matter content. The dry matter holding capacity is the ratio between the dry matter weight in rehydrated mushrooms and the sum of dry matter in rehydration liquid and rehydrated mushrooms [33].

The Box–Behnken design (BBD) was used to fit the relationship between rehydration kinetic parameters and VTCD processes. The experimental factors and levels of the VTCD processes were set as shown in Table 1. There were 17 drying and rehydration experiments, formed by 12 factorial points and 5 center points. The drying temperature increased from 308.15 K to 338.15 K in stages. The relative humidity was 30%, and the drying was completed when the shiitake mushroom's wet-basis moisture content was below 13%. In addition, the rehydration experiments of CTCD at 318.15 K and 338.15 K were supplemented.

Table 1. Factors and levels in BBD.

Factor (h)	−1 Level	0 Level	1 Level
A: Drying time at 308.15 K	2	4	6
B: Drying time at 318.15 K	2	4	6
C: Drying time at 328.15 K	2	4	6

A VTCD and two CTCD experiments were performed for drying model validation. For CTCD, the drying temperature (and relative humidity) were 333.15 K (20%) and 323.15 K (40%). For VTCD, the shiitake mushrooms were dried at 308.15 K, 318.15 K, and 328.15 K for 2 h, respectively, and then dried at 338.15 K until the drying process stopped. The wet-basis moisture content and volume shrinkage ratio of shiitake mushrooms during drying were calculated as Equations (1) and (2). Core temperatures were observed using needle-tip thermocouples inserted into the center of the shiitake mushrooms.

$$X_{wb,t} = \frac{m_t - m_0 \times (1 - X_{wb,0})}{m_t} \quad (1)$$

$$SR_{exp} = \frac{V_0 - V_t}{V_0} \quad (2)$$

where $X_{wb,t}$ and $X_{wb,0}$ represent the shiitake mushroom wet-basis moisture content at a specific time during drying and before drying; m_t and m_0 represent the shiitake mushroom mass at a specific time during drying and before drying, kg; SR_{exp} represents the experimental volume shrinkage ratio; V_t and V_0 represent the shiitake mushroom volume at a specific time during drying and before drying, m^3.

2.3. Variable-Temperature Convective Drying Numerical Model

Shiitake mushroom convective drying is multiphysical [34], as shown in Figure 2. Hot air is supplied continuously and flows through the ventilation chamber as a turbulent flow. The liquid water inside the mushroom evaporates and diffuses to the surface, driven by temperature and concentration gradients. The liquid water then diffuses into the air as water vapor. Dehydration and thermal expansion lead to structural deformation of the solid matrix, promoting the movement of liquid and vaporized water. The mushroom's

altered shape modifies the air flow rate and turbulence region, affecting the heat and mass transfer. The arbitrary Lagrangian–Eulerian method (ALE) models the interaction between turbulence flow and structural deformation, addressing the coupling between fluid and structure. Temperature affects the physical properties of air and water.

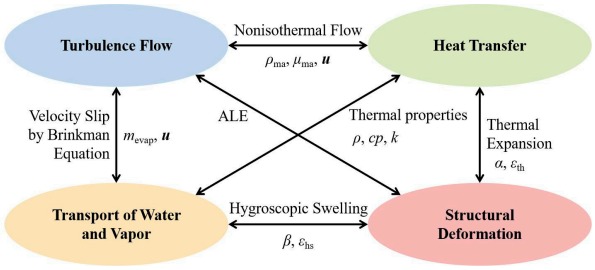


Figure 2. Multiphysics coupling in shiitake mushroom convective drying.

Since the drying process is complicated, assumptions are made to develop the VTCD model:

1. Shiitake mushroom is an unsaturated wet porous medium with uniform initial temperature and moisture content, having viscoelastic mechanical properties.
2. Moisture only leaves the mushroom as water vapor. There is no liquid water on the mushroom's surface.
3. Radiational, gravitational, and chemical energies are neglected.
4. The mushroom's mass change is caused only by moisture loss.
5. The model is based on the Cartesian coordinate system, simplifying the 3D drying process to a 2D representation to more efficiently study the relative effects of different drying conditions.

2.3.1. Governing Equations

The governing equations include moist air flow, energy, liquid water, and water vapor concentration, and stress–strain equations.

The Reynolds number is 19,505, according to the chamber size and air velocity. The algebraic turbulence model yPlus solves Reynolds-averaged Navier–Stokes (RANS) equations for momentum conservation (Equations (3) and (5)), a continuity equation for mass conservation (Equation (4)), and an algebraic equation for scaled wall distance (Equations (6)–(8)).

$$\rho_{ma}\frac{\partial \boldsymbol{u}}{\partial t} + \rho_{ma}(\boldsymbol{u}\cdot\nabla)\boldsymbol{u} = \nabla\cdot[-p\boldsymbol{I}+\boldsymbol{K}] \tag{3}$$

$$\frac{\partial \rho_{ma}}{\partial t} + \nabla\cdot(\rho_{ma}\boldsymbol{u}) = 0 \tag{4}$$

$$\boldsymbol{K} = (\mu_{ma}+\mu_T)\left(\nabla\boldsymbol{u} + (\nabla\boldsymbol{u})^T\right) - \frac{2}{3}(\mu_{ma}+\mu_T)(\nabla\cdot\boldsymbol{u})\boldsymbol{I} \tag{5}$$

$$Re_w = \frac{\rho_{ma}|\boldsymbol{u}|l_w}{\mu_{ma}} = \frac{|\boldsymbol{u}|}{u_\tau}\cdot\frac{\rho_{ma}u_\tau l_w}{\mu_{ma}} = u^+ l_w^+ u^+ = f\left(l_w^+\right) \tag{6}$$

$$\nabla G\cdot\nabla G + \sigma_w G(\nabla\cdot\nabla G) = (1+2\sigma_w)G^4 l_w = \frac{1}{G} - \frac{l_{ref}}{2} \tag{7}$$

$$\mu_T = \mu_{ma}\left(\left(\frac{df}{dl_w^+}\right)^{-1} - 1\right) \tag{8}$$

where ρ_{ma} is the moist air density, kg/m^3; $\boldsymbol{u}$ is the fluid velocity, m/s; p is the fluid pressure, Pa; $\boldsymbol{K}$ is the viscous stress tensor, Pa; μ_{ma} and μ_T are the moist air dynamic viscosity and turbulent viscosity, respectively, kg/(m·s); u_τ is the friction velocity, m/s; l_w is the wall distance, m; G is the reciprocal wall distance, 1/m; σ_w is the smoothing parameter.

The Brinkman equations are used in the porous media domain, as shown in Equations (9)–(11). The non-equilibrium approach explicitly speculates the evaporation rate, as shown in Equation (12) [35].

$$\frac{\rho_{ma}}{por_{sh} \times S_{ma}} \frac{\partial \boldsymbol{u}}{\partial t} + \frac{\rho_{ma}(\boldsymbol{u} \cdot \nabla)}{por_{sh} \times S_{ma}} \frac{\boldsymbol{u}}{por_{sh} \times S_{ma}} = \nabla \cdot [-p\boldsymbol{I} + \boldsymbol{K}] - \left(\frac{\mu_{ma}}{\kappa_{ma}} + \frac{C_F}{\sqrt{\kappa}} \rho_{ma} |\boldsymbol{u}| + \frac{Mn_l \cdot m_{evap}}{{por_{sh}}^2 \times {S_{ma}}^2} \right) \boldsymbol{u} \quad (9)$$

$$\frac{\partial (por_{sh} S_{ma} \rho_{ma})}{\partial t} + \nabla \cdot (\rho_{ma} \boldsymbol{u}) = Mn_l \cdot m_{evap} \quad (10)$$

$$\boldsymbol{K} = \frac{\mu_{ma}}{por_{sh} \cdot S_{ma}} \left(\nabla \boldsymbol{u} + (\nabla \boldsymbol{u})^T \right) - \frac{2}{3} \frac{\mu_{ma}}{por_{sh} \cdot S_{ma}} (\nabla \cdot \boldsymbol{u}) \boldsymbol{I} \quad (11)$$

$$m_{evap} = K(aw \times c_{v,sat} - c_v) por_{sh} S_{ma} \quad (12)$$

where por_{sh} is the mushroom porosity during shrinkage; S_{ma} is the gas phase saturation; κ_{ma} is the moist air permeability, m^2 [36]; C_F is the Forchheimer parameter, a dimensionless coefficient that accounts for the non-linear inertial effects in the flow through porous media at higher Reynolds numbers; κ is the absolute permeability of the porous medium; Mn_l is the liquid water molecular weight, kg/mol; m_{evap} is the evaporation rate, mol/(m^3·s); K is the non-equilibrium evaporation rate constant, 1/s; aw is the mushroom water activity [37]; $c_{v,sat}$ and c_v are the saturated vapor concentration and vapor concentration, mol/m^3.

The work performed by pressure changes and viscous dissipation in the fluid is ignored to simplify the energy equations. Equation (13) defines the temperature field of free airflow. Water vapor concentration affects the thermal characteristics of moist air, i.e., density, specific heat capacity, and thermal conductivity. The thermal convection velocity field utilizes the solution of the flow equation. The thermal properties in the cumulative and conduction terms of the porous media domain's energy equation are weighted by phase volume fractions. The thermal properties of the first convection term apply to liquid water and moist air in porous media. Moreover, the latent heat absorbed by liquid water evaporation is added as the source term, as defined by Equation (14).

$$\rho_{ma} cp_{ma} \frac{\partial T}{\partial t} + \rho_{ma} cp_{ma} \boldsymbol{u} \cdot \nabla T - \nabla \cdot (k_{ma} \nabla T) = 0 \quad (13)$$

$$\rho_{eff} cp_{eff} \frac{\partial T}{\partial t} + \rho_f cp_f \boldsymbol{u}_f \cdot \nabla T - \nabla \cdot (k_{eff} \nabla T) = -H \times Mn_l \times m_{evap} \quad (14)$$

where cp_{ma} is the moist air heat capacity, J/(kg·K); T is the temperature, K; k_{ma} is the moist air thermal conductivity, W/(m·K); ρ_{eff}, cp_{eff}, and k_{eff} are the effective volumetric density (kg/m^3), heat capacity (J/(kg·K)) and thermal conductivity (W/(m·K)) for all phases [37]; ρ_f, cp_f and $\boldsymbol{u}_f$ are the mobile fluid combined density (kg/m^3), heat capacity (J/(kg·K)), and velocity (m/s); H is the latent heat, J/kg.

Capillary suction is the basis for liquid water diffusion, and Darcy's law is used to determine convective transfer velocity. The promoting effect of solid shrinkage on liquid water mass transfer is considered. Liquid water decreases due to evaporation. Thus, Equation (15) represents the liquid water mass equation.

$$\frac{\partial c_l}{\partial t} + \nabla \cdot (-D_{cap} \nabla c_l) + \left(-\frac{\nabla p \times \kappa_l}{S_l \times por_{sh} \times \mu_l} \right) \cdot \nabla c_l + u_s \nabla c_l = -m_{evap} \quad (15)$$

where c_l is the liquid water concentration, mol/m^3; D_{cap} is the capillary diffusivity, m^2/s [38]; κ_l is the liquid water permeability, m^2 [36]; S_l is the liquid water saturation; μ_l is the liquid water viscosity, kg/(m·s).

Equations (16) and (17) represent water vapor transportation in porous media and air-free flow, respectively. Equation (18) illustrates that the water vapor diffusion in porous media is related to its diffusion coefficient in free air and the porous media porosity [39,40]. The convection term includes the water vapor migration caused by the moving velocity of the solid matrix [37]. Equation (19) expresses the diffusion coefficient's main determinants.

$$\frac{\partial c_v}{\partial t} + \nabla \cdot \left(-D_{eff} \frac{Mn_a}{Mn_{ma}} \nabla c_v \right) + \left(\frac{\boldsymbol{u}}{S_{ma} por_{sh}} - \frac{Mn_a D_{eff}}{Mn_{ma} \rho_{ma}} \nabla \rho_{ma} \right) \cdot \nabla c_v + u_s \nabla c_v = m_{evap} \tag{16}$$

$$\frac{\partial c_v}{\partial t} + \nabla \cdot (-D_{va} \nabla c_v) + \boldsymbol{u} \cdot \nabla c_v = 0 \tag{17}$$

$$D_{eff} = D_{va} \times por_{sh}^{\frac{4}{3}} S_{ma}^{\frac{10}{3}} \tag{18}$$

$$D_{va} = 2.2 \times 10^{-5} \times \frac{p_0}{p} \left(\frac{T}{T_0} \right)^{\frac{3}{2}} \tag{19}$$

where D_{eff} is the effective vapor diffusivity, m^2/s; Mn_a is the dry air molecular weight, kg/mol; D_{va} is the air-vapor diffusivity, m^2/s.

The shiitake mushroom displacements, mechanical stresses, and strains are computed using Equations (20)–(25).

$$\rho_{eff} \frac{\partial^2 \boldsymbol{U}}{\partial t^2} = \nabla \cdot (F\sigma)^T, \; F = I + \nabla U \tag{20}$$

$$\sigma = \sigma_{inel} + J_i F_{inel}^{-1} (C : \varepsilon_{el}) F_{inel}^{-T}, \; \varepsilon_{el} = \frac{1}{2} \left(F_{el}^T F_{el} - I \right), F_{el} = F F_{inel}^{-1} \tag{21}$$

$$\sigma_{inel} = \sigma_0 + \sigma_{ext} + \sigma_q \tag{22}$$

$$\varepsilon = \frac{1}{2} \left[(\nabla \boldsymbol{U})^T + \nabla \boldsymbol{U} + (\nabla \boldsymbol{U})^T \nabla \boldsymbol{U} \right] \tag{23}$$

$$\boldsymbol{C} = \boldsymbol{C}(E, \boldsymbol{\nu}) \tag{24}$$

$$\rho_{eff} = \rho_s (1 - por_{sh}) + \rho_l por_{sh} S_l + \rho_{ma} por_{sh} S_{ma} \tag{25}$$

where $\boldsymbol{U}$ is the structural displacement, m; F is the deformation gradient tensor; σ is the second Piola–Kirchhoff stress, Pa; ε_{el} is the elastic strain; σ_0, σ_{ext}, and σ_q are the initial stress, external stress, and viscoelastic stress, respectively, Pa; $\boldsymbol{C}$ is the constitutive tensor; E is the elastic modulus, Pa; ν is the Poisson's ratio.

Ignoring the effects of shrinkage on heat and mass transfer reduces simulation accuracy [41]. However, the linear elastic model is only valid for small deformations [42]. The generalized Maxwell model for viscoelastic material is the most common method for predicting the stress–strain relationship during drying of different foods, such as strawberries [43], carrots [44], and pumpkins [45]. The stress relaxation curves of shiitake mushrooms [46] are used to model the relationship between generalized Maxwell parameters and drying conditions, which is provided in the Supplementary Materials.

The total strain also includes thermal and hygroscopic strains, defined by Equations (26) and (27), respectively. Equation (28) determines the hygroscopic expansion coefficient by fitting experimental data.

$$\varepsilon_{th} = \alpha(T)(T - T_{ref}) \tag{26}$$

$$\varepsilon_{hs} = \beta Mn_l \left(c_l - \frac{S_{l,0} \times por_{sh} \times \rho_l}{Mn_l} \right) \tag{27}$$

$$\beta = 9 \times 10^{-4} \ln(15 + X_{db}) \tag{28}$$

where ε_{th} and ε_{hs} are the thermal strain and hygroscopic strain; α is the thermal expansion coefficient, 1/K; T_{ref} is the reference temperature, K; β is the hygroscopic expansion coefficient, m^3/kg; X_{db} is the dry basis moisture content.

2.3.2. Initial and Boundary Conditions

The model parameters are listed in Table 2. The non-equilibrium evaporation rate constant K depends on the ambient fluid, the convective heat transfer coefficient, etc. While

independent methods of measuring K for a hygroscopic material are still lacking, pure water evaporation was estimated to be of the order of 1 1/s [47,48]. The drying process lowers moisture content while increasing glass transition temperature. However, shiitake mushrooms with 15% wet-basis moisture content have a glass transition temperature below −40 °C [49], much lower than the drying temperature. Therefore, shiitake mushrooms are rubbery and show viscoelastic behaviors during drying. The Poisson's ratio is taken as 0.49 according to [22]. The initial water saturation is calculated from the initial moisture content, solid matrix density, and liquid water density [50]. The initial conditions are listed in Table 3.

Table 2. Parameters of the drying model.

Parameter	Value	Unit	Description
cp_s	1500 [51]	J/(kg·K)	Solid matrix heat capacity
E_m	4×10^5 [50]	Pa	Mushroom elastic modulus
H	2.37055×10^6	J/kg	Evaporation latent heat
K	1	1/s	Non-equilibrium evaporation rate constant
k_s	0.1 [51]	W/(m·K)	Solid matrix thermal conductivity
p_0	101,325	Pa	Ambient pressure
RH_0	0.8	-	Ambient relative humidity
S_{il}	0.05 [38]	-	Irreducible liquid phase saturation
$S_{l,0}$	0.62	-	Initial water saturation
T_0	293.15	K	Ambient temperature
u_{in}	3.0	m/s	Freestream velocity
por	0.95 [50]	-	Initial porosity
α	2.5×10^{-6} [50]	1/K	Thermal expansion coefficient
κ	1×10^{-14}	m^2	Absolute permeability of shiitake mushroom
ν	0.49	-	Poisson's ratio
ρ_s	1591 [50]	kg/m^3	Solid matrix density

Table 3. Initial conditions.

Physical Quantity	Porous Medium Domain	Air Free Flow Domain	Description
U	0	0	Velocity
P	0	0	Pressure
T	T_0	T_0	Temperature
$c_{l,0}$	$S_{l0} \times por \times \rho_l / Mn_l$	0	Liquid water concentration
$c_{v,0}$	$c_{v,sat,0} \times (1 - S_{l,0}) \times por$	$c_{v,sat,0} \times RH_0$	Water vapor concentration
U	0	-	Displacement
$\frac{\partial U}{\partial t}$	0	-	Structural velocity

The Dirichlet boundary condition is adopted at the inlet of the ventilation chamber. The inlet flow is fully developed, where the average air state parameters (temperature, relative humidity, and air velocity) are consistent with the drying conditions. A piecewise function, as shown in Figure 3, defines the drying temperature of VTCD for drying characteristics analysis. The shiitake mushroom is dried at 308.15 K, 318.15 K, and 328.15 K for 2.4 h, 3.3 h, and 5.6 h, respectively, and then dried at 338.15 K until the moisture content reaches 13% [17]. The temperature curve is smoothed using the continuous second derivative. The ventilation chamber walls are no-slip, adiabatic, and have no mass flux. The outlet relative pressure is 0 Pa. There are no liquid water flux and load constraints on mushroom's boundaries.

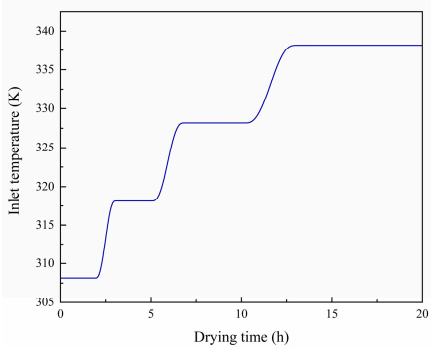


Figure 3. VTCD for drying characteristics analysis.

2.3.3. Numerical Solution

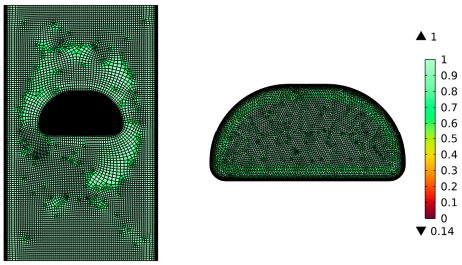
The model is solved using COMSOL Multiphysics software. The turbulent flow algebraic yPlus, heat transfer in fluids, transport of diluted species, and solid mechanics interfaces are used to compute the velocity and pressure, temperature, concentration of water vapor and liquid water, and strain inside the shiitake mushroom, respectively. Furthermore, the non-isothermal flow multiphysics coupling is used to simulate fluid flows whose properties are temperature-dependent. Moreover, thermal expansion and hygroscopic swelling multiphysics coupling are added to simulate the internal strain caused by temperature and moisture changes. The solver stops when the average wet base moisture content is less than 13%. In each time step, the solutions are assumed to be converged when the relative toleration is less than 0.01.

Mesh independence study is an essential step in numerical simulation. Three grids are tested for key variables, relative errors, and grid convergence indices (GCI) [52]. The wet-basis moisture content after 10 h VTCD drying is used as the key variable. As shown in Table 4, both GCI_{12} and GCI_{23} are less than 5%. Grid2 is used to solve the model in order to save computing time.

Table 4. Grid convergence test.

Grid	Number of Cells	Wet-Basis Moisture Content	Relative Error	GCI
1	12,645	0.46219		
2	20,633	0.46147	0.0016	0.0030
3	50,163	0.45735	0.0090	0.0075

As shown in Figure 4, the meshing is built using the COMSOL predefined "free quadrilateral" with an "extra fine" mesh element size for the air-free flow region and "free triangular" with a "extremely fine" mesh element size for the porous medium domain, calibrated for fluid dynamics. Eight boundary layers are added to the border of the mushroom and chamber walls (adjustment factor 1.2). A moving mesh governs the space frame, and the air-free flow domain is designated as the deformation domain. In the transient study, select automatic remeshing to prevent mesh cell inversion and maintain mesh quality, ensuring calculation stability and accuracy.



(**a**) Free airflow (**b**) Porous media

Figure 4. Numerical meshing. (The color legend refers to the skewness in the grid cell quality).

2.4. Shiitake Mushroom Rehydration Model after Variable-Temperature Convective Drying

2.4.1. Rehydration Kinetics Modelling

Peleg [53] proposed a two-parameter, nonexponential empirical model to fit sorption curves for rice soaked in water. This model has been widely used to describe the rehydration behavior of food during different drying processes [54–56], and it fits well with the experimental data of rehydration kinetics of dried edible fungi, such as boletus edulis mushroom [57], morel [58], and shiitake mushroom [27]. Therefore, Peleg model is used to describe the rehydration kinetics of shiitake mushrooms after VTCD:

$$X_{db,t} = X_{db,d} + \frac{t}{K_1 + K_2 \times t} \tag{29}$$

where $X_{db,t}$ and $X_{db,d}$ are the dry basis moisture content during and before rehydration, respectively; t is the rehydration time, min; K_1 is the Peleg rate constant, min; K_2 is the Peleg capacity constant.

2.4.2. Rehydration Indices

Rehydration comprises three simultaneous processes: the imbibition of water into dried material, the swelling of the rehydrated products, and the leaking of soluble solids [59]. Because the rehydration ratio measures the relative mass increase in dried material rehydrated in water, it provides no information regarding the matrix's ability to recover water lost during drying. Therefore, the rehydration ratio cannot be used to explain the material's rehydration characteristics after drying individually. Lewicki [60] proposed three indices to calculate the rehydration ability of dried foods. The water absorption capacity (WAC), dry matter holding capacity (DHC), and rehydration ability (RA) are calculated as follows:

$$WAC = \frac{m_r(1 - s_r) - m_d(1 - s_d)}{m_0(1 - s_0) - m_d(1 - s_d)} \tag{30}$$

$$DHC = \frac{m_r s_r}{m_d s_d} \tag{31}$$

$$RA = WAC \cdot DHC \tag{32}$$

where m and s represent a sample's mass and percent dry matter content (0, d, r–initial, dried, rehydrated).

2.4.3. Relationship with Drying Numerical Model

First, the connection between VTCD processes and shiitake mushroom's rehydration kinetics is established. The rehydration calculation module is then added to the shiitake mushroom VTCD numerical model, creating a mathematical model combining drying and rehydration. This integration enables the examination of the gradient change in drying characteristics (difficult to measure in experiments) and its relationship to rehydration effectiveness, as well as the demonstration of VTCD technology's advantages. The derivation of the formula is shown in Appendix A.

2.5. Statistical Analysis

Origin 2018 and Design Expert 11 were used for statistical analysis. Drying and rehydration experiments were conducted in triplicate. The drying model's accuracy was evaluated using statistical indicators, including the coefficient of determination (R^2), root mean square error (RMSE), and mean absolute error (MAE). Non-linear regression analysis of the experimental data was conducted to obtain the kinetic parameters K_1 and K_2 of shiitake mushroom rehydration processes after different VTCD processes. Statistical parameters include standard error (SE), reduced chi-square (χ^2), and adjusted R-square (Adj. R^2). Analysis of variance (ANOVA) for the model of the Peleg rate constants was employed to identify significant differences ($p < 0.05$). Further, a polynomial relationship between rehydration kinetic parameters and drying time at each temperature in VTCD processes is obtained. The calculation and meanings of the statistical parameters are provided in the Supplementary Materials.

3. Results and Discussion

3.1. Dehydration Characteristics

3.1.1. Drying Model Validation

Figure 5 shows the numerical and experimental results of the wet-basis moisture content, volume shrinkage ratio, and core temperature of the shiitake mushroom. The numerical results of the drying model are very close to the experimental results. The average coefficients of determination (R^2) are 0.9936, 0.9285, and 0.8729 for the wet-basis moisture content, volume shrinkage ratio, and core temperature, respectively. The mean absolute errors (MAEs) are 0.0226, 0.0880, and 2.9494 K for the wet-basis moisture content, volume shrinkage ratio, and core temperature, respectively. Moreover, the root mean square errors (RMSEs) are 0.0383, 0.1079, and 3.6849 K for the wet-basis moisture content, volume shrinkage ratio, and core temperature, respectively. Accordingly, this model simulates the shiitake mushroom convective drying process accurately. This model investigates the shiitake mushroom dehydration and drying load characteristics during VTCD.

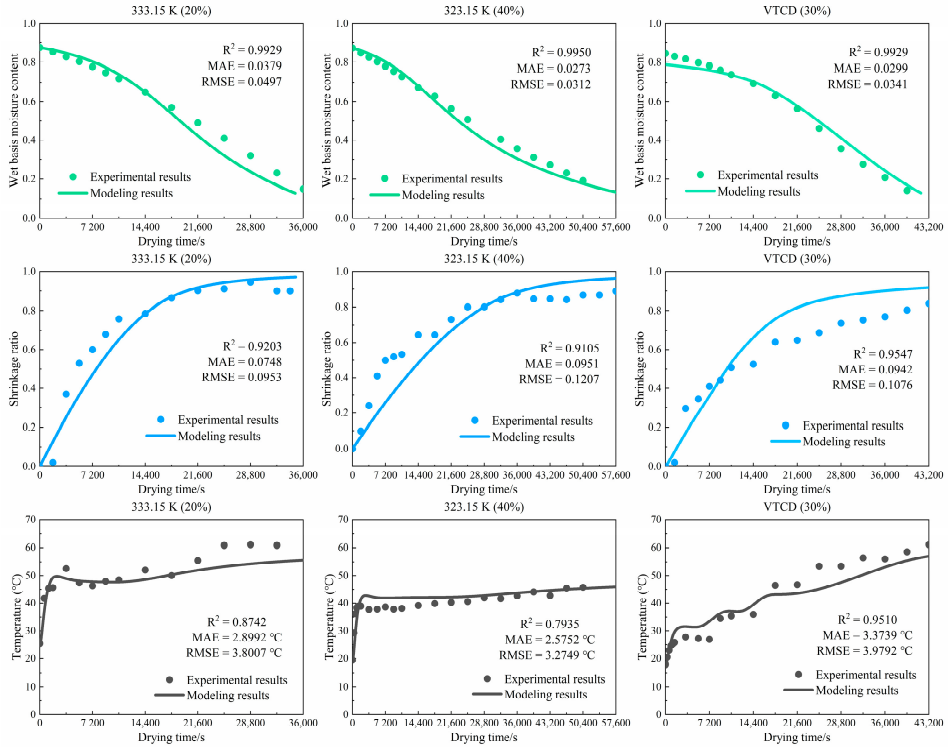
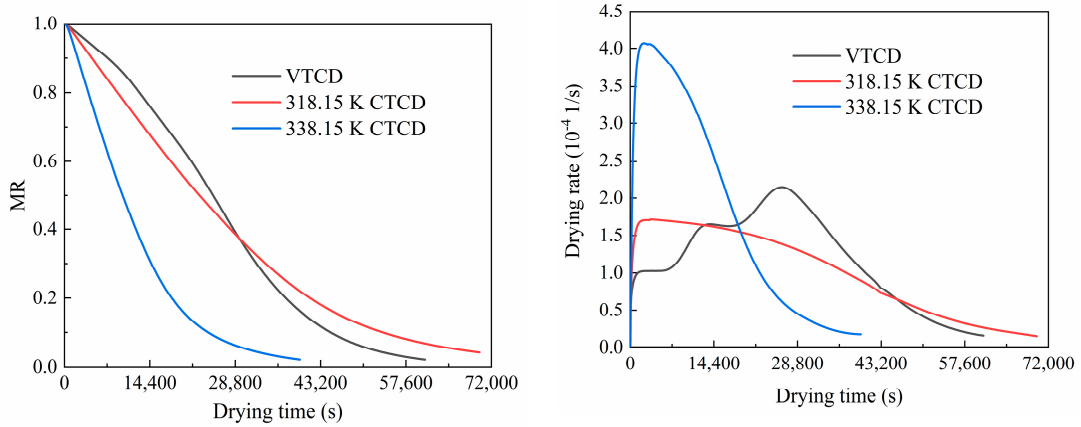


Figure 5. Experimental and numerical results of the wet-basis moisture content, volume shrinkage ratio, and core temperature under different shiitake mushroom drying processes.

3.1.2. Moisture Ratio and Drying Rate of Shiitake Mushrooms

In industrial applications, the temperature for CTCD of shiitake mushrooms typically ranges from 318.15 K to 338.15 K for efficient moisture removal while preserving quality. Therefore, the numerical model simulates a VTCD process and two CTCD processes at 318.15 K and 338.15 K. In the VTCD process, drying occurs at 308.15 K, 318.15 K, and 328.15 K for 2.4 h, 3.3 h, and 5.6 h, respectively, before continuing at 338.15 K until completion [17]. The drying relative humidity is 30%. MR is an important dimensionless parameter to quantify variation in the moisture content of shiitake mushrooms during drying. The drying rate refers to the derivative of dry basis moisture content with respect to time. As illustrated in Figure 6, although the MRs of the three drying processes all decrease from 1 to about 0.03, the MR of the VTCD process shows the lowest decreasing rate at the early drying stage and is the largest in the first eight hours.



(**a**) MR (**b**) Drying rate

Figure 6. MR and drying rate of shiitake mushrooms in VTCD and CTCD processes.

Furthermore, the drying rates of the two CTCD processes increase sharply at the early drying stage and decrease continuously after reaching the peak. A higher drying air temperature results in a faster drying rate and a shorter drying time. This is due to increased ambient heat supply to the product and accelerated water mobility within the mushroom. These findings are consistent with the literature on drying [16]. Meanwhile, the drying rate of the VTCD process is relatively steady. Although the final drying temperature of VTCD reaches 338.15 K, the maximum drying rate (0.0002 1/s) is about half that of 338.15 K CTCD (0.00041 1/s), which is close to the 318.15 K CTCD (0.00017 1/s).

3.1.3. Temperature of Shiitake Mushrooms

Figure 7 illustrates the core temperature and temperature gradient. The bottom of the shiitake mushroom reaches the drying temperature the fastest, so the initial temperature gradient during drying is approximately the difference between the drying temperature and the ambient temperature. There are apparent temperature gradients inside the shiitake mushroom in the CTCD processes. As heat is transferred to the interior of the shiitake mushroom, the temperature gradient of the mushroom decreases rapidly, but it still maintains relatively high during the initial drying stage (the temperature gradients of 338.15 K CTCD, 318.15 K CTCD, and VTCD can reach 10.41 K, 7.68 K, and 3.12 K, respectively). For CTCD, the core temperatures rise rapidly in the first hour, approach their drying temperatures, and then drop slightly. The reason is that the evaporation rate in the internal region is significant, and the heat consumed by evaporation exceeds that transferred from the surface. The evaporation rate slows down in the middle of drying, and the temperature inside the mushroom rises again. Two hours after the start of drying, the temperature gradient of CTCD gradually decreases. However, the temperature rises uniformly in the VTCD process, and the shiitake mushroom temperature gradient is relatively small and

stable. Since the endpoint of the drying experiment is a wet-basis moisture content of 13% rather than 0%, moisture evaporation and heat absorption continue throughout the process. Consequently, the core temperatures of the shiitake mushrooms remain below the drying temperatures. The shiitake mushroom temperature distribution in the VTCD and CTCD processes after drying for 1, 4, and 8 h and at the last moment are displayed in Appendix B.

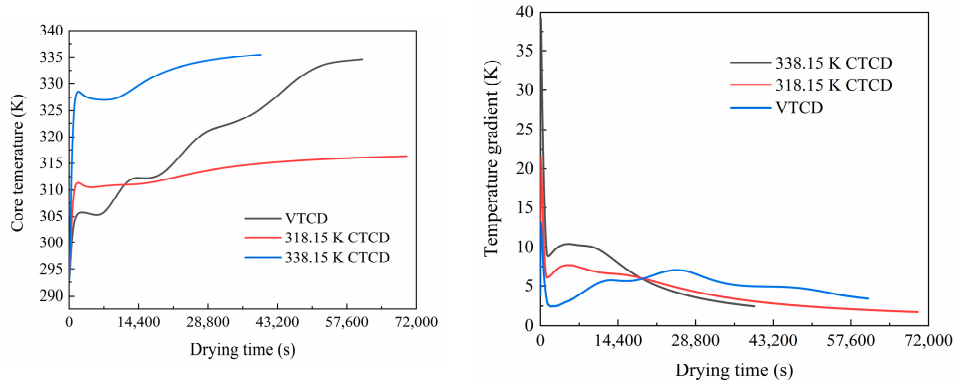


Figure 7. Core temperature (**a**) and temperature gradient (**b**) of shiitake mushrooms in VTCD and CTCD processes.

3.1.4. Evaporation Rate of Shiitake Mushrooms

The average evaporation rates (molar amount of evaporation water per unit volume and unit time) and evaporation gradients are shown in Figure 8. The evaporation rate changes considerably in the CTCD processes. In the early drying stage, the evaporation rate of VTCD is the lowest. The peak average evaporation rates of 338.15 K CTCD, 318.15 K CTCD, and VTCD reach 0.73, 0.39, and 0.71 mol/(m^3·s), respectively, while the peak evaporation rate gradients reach 2.24, 0.92, and 1.50 mol/(m^3·s), respectively. Therefore, VTCD can simultaneously achieve a high and low evaporation rate gradient in the later drying stages. During drying at increasing temperatures, the stimulations during temperature changes generate an acceleration of the phenomena of evaporation, which is also found in spearmint [16]. The distribution of shiitake mushroom evaporation rate in the VTCD and CTCD processes is shown in Appendix B. The results show that the variation in the evaporation rate in the VTCD process is the smallest at the early stage. Water evaporation mainly occurs in the external region of the shiitake mushroom, exhibiting a significantly higher evaporation rate than the internal region. The evaporation rate in the external region gradually decreases with the decrease in moisture content.

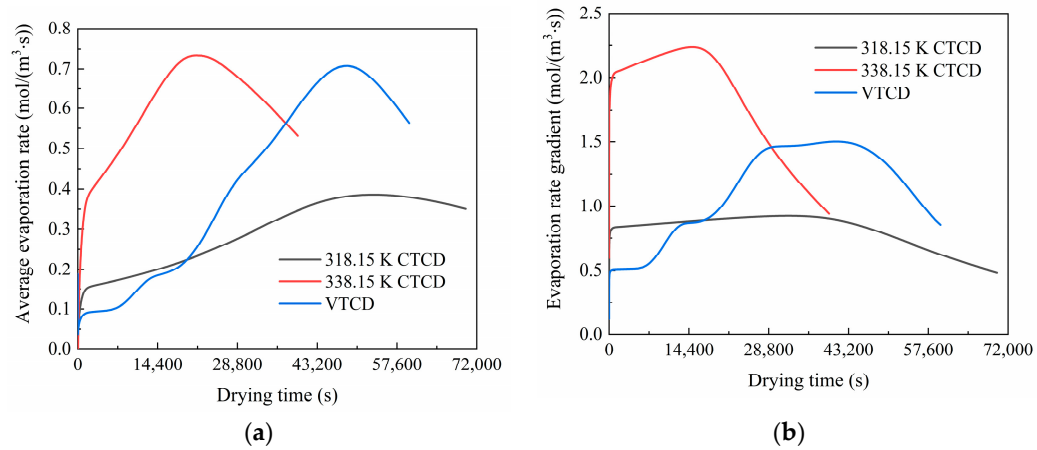


Figure 8. Average evaporation rate (**a**) and evaporation rate gradient (**b**) of shiitake mushrooms in VTCD and CTCD processes.

3.1.5. Volume Shrinkage Ratio of Shiitake Mushrooms

The shrinkage ratio of shiitake mushrooms in the VTCD and CTCD processes are compared by calculating their volumetric strain, as displayed in Figure 9. The shrinkage ratios increase gradually and are more than 0.9 at the final dried state. Although the shrinkage ratio of the VTCD process is moderate after drying, it maintains the smallest for the first eight hours. It is noted that increased shrinkage ratios can reduce rehydration capacity because of surface cracking, a phenomenon that becomes apparent during the drying process [61]. Therefore, VTCD can mitigate this impact.

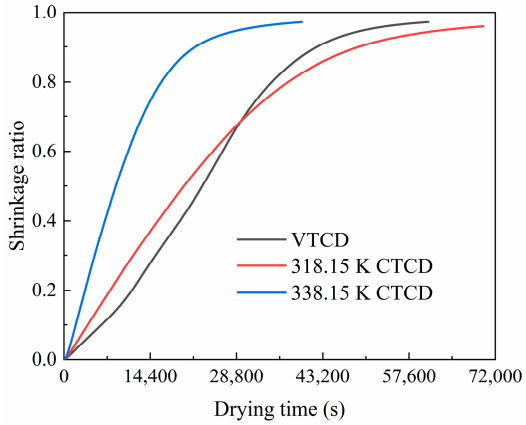


Figure 9. Shrinkage ratio of shiitake mushrooms in VTCD and CTCD processes.

3.1.6. Enthalpy Difference between the Inlet and Outlet of the Drying Chamber

The humid air enthalpy is integrated into the inlet and outlet boundary to compare heat and moisture loads of the drying chamber in VTCD and CTCD processes. The drying load in kW/m represents the energy transfer rate per unit width in the 2D plane, which is consistent with the Cartesian coordinate system. This unit is used because the simulation represents a vertical 2D slice of the drying chamber. The energy transfer rate for the entire system can be obtained by integrating over the width or applying a suitable geometric correction if necessary. This approach is used for relative comparisons under different drying conditions. The enthalpy flow curves changing with drying time are shown in Figure 10. The total drying time of the VTCD process is between those of the two CTCD processes. The drying load of the VTCD process shows better stability compared to those of CTCD processes, especially at the early drying stage. The maximum drying loads are 19.24 kW/m (338.15 K CTCD), 9.93 kW/m (318.15 K CTCD), and 7.92 kW/m (VTCD), respectively. The maximum drying load of VTCD is 41.16% of that of 338.15 K CTCD. The VTCD process exhibits the narrowest range of heat and moisture load fluctuations, which is advantageous for the steady and energy-efficient operation of energy supply equipment like heat pumps.

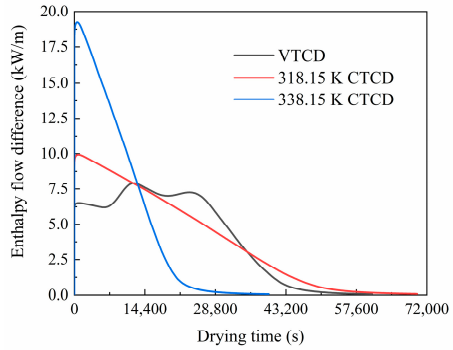
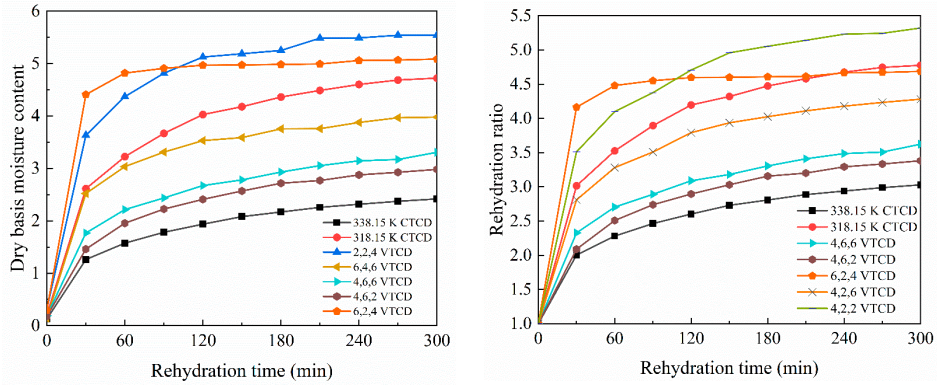


Figure 10. Air enthalpy difference between the inlet and outlet of the drying chamber in VTCD and CTCD processes.

3.2. Rehydration Processes

3.2.1. Rehydration Kinetics after Variable-Temperature Convective Drying

Figure 11a,b show the experimental rehydration kinetics of shiitake mushrooms after different drying processes. The numbers before 'VTCD' in the legend represent the drying time at 308.15 K, 318.15 K, and 328.15 K, respectively. Two CTCD processes and thirteen VTCD processes are performed, as described in Section 2.2. For the simplicity of the graphical display, only five representative VTCD data points are retained, and the other eight sets of results are close to that of 318.15 K CTCD. Within the first 30 min of rehydration, all mushrooms absorb water rapidly, which raises the dry basis moisture contents. Over the next several hours, the water absorption rates gradually decrease until the equilibrium moisture contents are reached. Surface and capillary suction are the main causes of the first stage's rapid moisture absorption.



(**a**) Dry basis moisture content (**b**) Rehydration ratio

Figure 11. Experimental results of rehydration kinetics of shiitake mushrooms under different drying processes.

Upon wetting, the surface moisture concentration rises to saturation immediately, and moisture movement is restricted within the material [62]. The driving force for water transfer diminishes as the rehydration process approaches equilibrium [63]. The initial moisture contents of shiitake mushrooms are unknown during drying experiments because they are determined by drying the mushrooms and rehydration solution to constant weight after rehydration experiments. The end of the drying experiments is estimated according to the assumed 85% moisture content dried to 13%, resulting in inaccurate moisture contents after drying. After 300 min of rehydration, the shiitake mushrooms' dry basis moisture contents rise from 0.13–0.31 to 2.42–5.54. Among all the drying processes, mushrooms dried at 338.15 K have the lowest dry basis moisture content. The rehydration ratios under various drying processes follow a similar trend to the dry base moisture contents. The rehydration ratios under different drying processes increase from 1 to 3.03–5.32 after rehydration. The rehydration ratio of the shiitake mushroom dried at 338.15 K is the smallest, and the rehydration ratio of the shiitake mushroom dried at 318.15 K is among that of shiitake mushrooms dried under different VTCD processes. The rehydration ratios of VTCD exceed 2 within 30 min of rehydration, and similar results have been obtained in the literature [29]. The rehydration speed of shiitake mushrooms after VTCD is fast during the initial rehydration stage, possibly due to the porous structure and low shrinkage rate of the mushrooms. Similar findings have also been reported in the literature [64].

The initial moisture contents of mushroom samples range from 4.58 to 7.61 due to the individual variances in shiitake mushrooms. Combined with Figure 11a and Table 5, the dry basis moisture contents after rehydration are all lower than the initial moisture contents, indicating irreversible cell damage and dislocation during the drying process. The significant shrinkage of the capillary and collapse of the dense tissue structure reduce hydrophilicity, so it cannot wholly absorb enough water [26]. Since the mushroom samples'

initial properties cannot be entirely consistent, it is difficult to eliminate the interference of different initial properties in the rehydration experimental results. Therefore, a numerical model combining drying and rehydration is established, which unifies the material properties and is used to analyze the effect of VTCD processes on mushroom rehydration performance.

Table 5. Experimental results of initial dry basis moisture content and DHC after rehydration.

Drying Processes	Initial Dry Basis Moisture Content	DHC
6,4,6 VTCD	4.58 ± 0.52	0.76 ± 0.02
4,6,2 VTCD	4.75 ± 0.81	0.69 ± 0.02
4,6,6 VTCD	4.75 ± 0.47	0.71 ± 0.04
6,6,4 VTCD	5.10 ± 0.59	0.77 ± 0.002
338.15 K CTCD	5.31 ± 0.84	0.75 ± 0.05
2,6,4 VTCD	5.77 ± 0.44	0.79 ± 0.06
4,2,6 VTCD	5.78 ± 1.33	0.81 ± 0.06
4,4,4 VTCD	6.04 ± 1.15	0.79 ± 0.01
2,2,4 VTCD	6.31 ± 1.51	0.75 ± 0.06
2,4,2 VTCD	6.73 ± 1.63	0.73 ± 0.03
318.15 K CTCD	6.86 ± 1.18	0.77 ± 0.06
6,4,2 VTCD	6.92 ± 1.14	0.80 ± 0.02
4,2,2 VTCD	7.38 ± 1.38	0.79 ± 0.05
2,4,6 VTCD	7.54 ± 0.32	0.75 ± 0.01
6,2,4 VTCD	7.61 ± 0.62	0.78 ± 0.02

Because the dry matter content determination is a destructive analysis [65], the time-dependent solid leakage rate during rehydration is unknown, and only the DHC is measured after rehydration. According to Table 5, the DHCs of rehydrated shiitake mushrooms under different drying processes are close and high (the average DHC is 0.77). Therefore, solid leakage is eventually not considered.

3.2.2. Rehydration Model Related to Variable-Temperature Convective Drying Conditions

The Peleg equation (Equation (29)) is applied to the experimental data of the rehydration curve. Table 6 shows the K_1 and K_2 values for dried shiitake mushrooms under different drying conditions. The adjusted R-square values vary from 0.9906 to 0.9994, while reduced Chi-square values range from 0.0012 to 0.0125. These values indicate an excellent concordance with the experimental data, implying that Peleg's model could reasonably describe the rehydration kinetics of shiitake mushrooms under examined conditions.

The Peleg rate constant K_1 relates to the initial water absorption rate, and its reciprocal can be likened to a diffusion coefficient [66]. The lower the K_1, the higher the water absorption rate at the beginning of rehydration. Table 6 shows that K_1 ranges from 1.05 to 17.71 min under the 19 drying processes. Shiitake mushrooms dried at 338.15 K have the highest K_1, indicating the lowest water absorption rate during rehydration. The Peleg capacity constant K_2 refers to the maximum attainable moisture content during rehydration, i.e., equilibrium moisture content [67]. Under experimental drying conditions, K_2 is between 0.18 and 0.39. Although the 338.15 K CTCD process has the shortest total drying time, the moisture content is the lowest when rehydration reaches equilibrium. This is because the high temperature throughout the drying process causes intensive structural changes and reduces the extent of rehydration.

Table 6. Peleg constants for the rehydration of dried shiitake mushrooms under different drying conditions.

RUN	Drying Process	A Drying Time at 308.15 K (h)	B Drying Time at 318.15 K (h)	C Drying Time at 328.15 K (h)	K_1 (min)	Standard Error	K_2	Standard Error	Reduced Chi-Sqr	Adj. R-Square
1	VTCD	4	6	2	15.29	0.55	0.31	0.0037	0.0013	0.9981
2		4	4	4	6.98	0.67	0.27	0.0054	0.0097	0.9906
3		2	4	2	5.16	0.18	0.22	0.0015	0.0018	0.9988
4		4	2	6	7.76	0.42	0.23	0.0032	0.0047	0.9965
5		2	4	6	4.17	0.19	0.21	0.0017	0.0030	0.9983
6		6	4	2	5.48	0.24	0.21	0.0019	0.0034	0.9980
7		4	4	4	6.79	0.47	0.25	0.0037	0.0059	0.9950
8		6	2	4	1.05	0.06	0.21	0.0007	0.0012	0.9994
9		6	4	6	5.73	0.32	0.25	0.0027	0.0036	0.9971
10		4	4	4	4.43	0.38	0.24	0.0034	0.0076	0.9943
11		2	2	4	3.86	0.14	0.18	0.0012	0.0028	0.9988
12		4	2	2	5.31	0.32	0.18	0.0025	0.0092	0.9959
13		4	4	4	4.92	0.33	0.22	0.0028	0.0062	0.9959
14		4	6	6	12.00	0.93	0.29	0.0066	0.0064	0.9920
15		2	6	4	9.03	0.53	0.20	0.0037	0.0081	0.9952
16		6	6	4	5.84	0.39	0.22	0.0031	0.0068	0.9955
17		4	4	4	6.00	0.50	0.21	0.0039	0.0125	0.9926
18	CTCD		318.15 K		7.37	0.37	0.20	0.0027	0.0058	0.9968
19			338.15 K		17.71	1.15	0.39	0.0079	0.0027	0.9940

Table 7 shows the ANOVA result for the reduced quadratic model of Peleg rate constant K_1. The model F-value of 16.25 implies the model is significant. There is a 0.01% chance that an F-value this large is caused by noise. *p*-values less than 0.05 indicate that model terms are significant. B, BC, A^2, B^2, C^2 are significant terms. B, i.e., drying time at 318.15 K, is the most critical factor affecting the Peleg rate constant K_1 of shiitake mushrooms during rehydration. The model's significance and adequacy are collaborated by the coefficient of determination (R^2) of 0.91. As reported in Table 8, an F value of 7.91 implies that the model for K_2 is significant. The chance that the F value is caused by noise is 0.42%. B, A^2, and A^2B are significant model terms. B, i.e., the drying time at 318.15 K, is the most critical factor affecting K_2. R^2 (0.89) collaborates on the significance and adequacy of the model.

Table 7. ANOVA for the reduced quadratic model of the Peleg rate constant K_1.

Source	Sum of Squares	df	Mean Square	F-Value	*p*-Value	
Model	154.22	6	25.70	16.25	0.0001	significant
A—Drying time at 308.15 K	2.11	1	2.11	1.33	0.2753	
B—Drying time at 318.15 K	73.03	1	73.03	46.16	0.0001	
BC	8.24	1	8.24	5.21	0.0456	
A^2	35.82	1	35.82	22.64	0.0008	
B^2	17.47	1	17.47	11.04	0.0077	
C^2	20.83	1	20.83	13.17	0.0046	
Residual	15.82	10	1.58			
Lack of Fit	10.77	6	1.79	1.42	0.3826	not significant
Pure Error	5.05	4	1.26			
Cor Total	170.04	16				

Table 8. ANOVA for the reduced cubic model of the Peleg capacity constant K_2.

Source	Sum of Squares	df	Mean Square	F-Value	*p*-Value	
Model	0.0184	8	0.0023	7.91	0.0042	significant
A—Drying time at 308.15 K	0.0006	1	0.0006	2.13	0.1824	
B—Drying time at 318.15 K	0.0092	1	0.0092	31.46	0.0005	
C—Drying time at 328.15 K	0.0004	1	0.0004	1.42	0.2679	
AC	0.0007	1	0.0007	2.46	0.1551	
BC	0.0012	1	0.0012	4.05	0.0790	
A^2	0.0049	1	0.0049	16.84	0.0034	
C^2	0.0013	1	0.0013	4.51	0.0664	
A^2B	0.0029	1	0.0029	9.94	0.0136	
Residual	0.0023	8	0.0003			
Lack of Fit	0.0001	4	0.0000	0.06	0.9904	not significant
Pure Error	0.0022	4	0.0005			
Cor Total	0.0208	16				

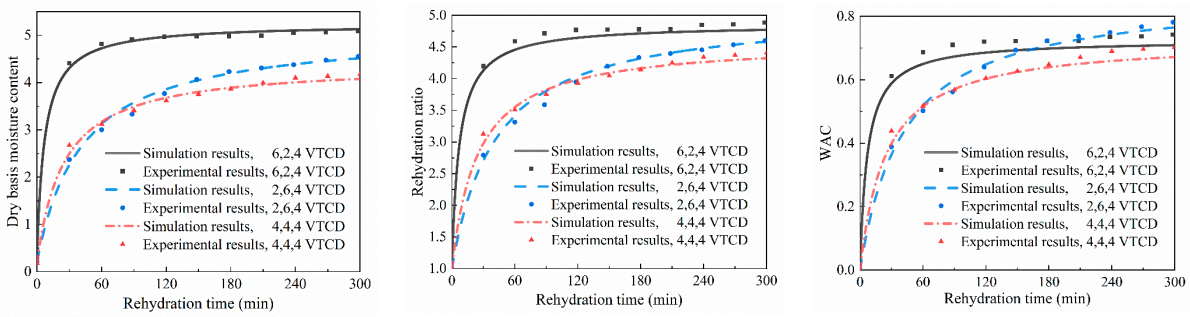
The equation in terms of coded factors is used to predict the response for given levels of each factor. High levels (+1) and low levels (−1) of the factors (A, B, and C) are assigned by default. The coded equation helps identify the relative impacts of factors based on their coefficients. The equations for K_1 and K_2 in terms of coded factors are given by Equations (33) and (34). They establish the connection between VTCD processes and rehydration kinetics.

$$K1 = 5.82586 - 0.51325 \times A + 3.02139 \times B - 1.4353 \times BC - 2.91671 \times A^2 + 2.03687 \times B^2 + 2.22422 \times C^2 \quad (33)$$

$$\begin{aligned} K2 = {} & 0.236811 + 0.0088125 \times A + 0.047875 \times B + 0.0071875 \times C \\ & + 0.0134 \times AC - 0.017175 \times BC - 0.0340987 \times A^2 + 0.0176513 \times C^2 - 0.03805 \times A^2B \end{aligned} \quad (34)$$

3.2.3. Validation of the Numerical Rehydration Model

Representative experiments are selected to verify the rehydration model's accuracy. Since the initial conditions significantly affect the experimental results, the model's input parameters (including ambient conditions, drying conditions, and the mushroom moisture content before and after drying) are expressed using the values obtained from corresponding experiments. Figure 12 compares the simulated and experimental rehydration performance, including dry basis moisture content, rehydration ratio, and WAC. The results show that the model results agree with the actual situation. Therefore, the initial conditions, except drying processes, are unified in the model, and the comprehensive influence of VTCD processes on rehydration performance and drying time is analyzed.



(**a**) Dry basis moisture content (**b**) Rehydration ratio (**c**) WAC

Figure 12. Comparison between simulated and experimental results for rehydration.

3.2.4. Assessment of Rehydration after Variable-Temperature Convective Drying

Shiitake mushroom enzymatic and non-enzymatic reactions are primarily influenced by drying temperature and drying time [11], and WAC is related to chemical composition [62]. Therefore, shiitake mushroom WACs are simulated using different VTCD processes. Figure 13 illustrates how VTCD processes affect WAC and total drying time. The simulation input parameters are the same as those in Table 2. The results show that, among the 13 VTCD processes, the highest WAC is 0.74 (2,2,4 VTCD), and the lowest WAC is 0.31 (4,6,2 VTCD), while the longest total drying time is 19.51 h (6,6,4 VTCD), and the shortest is 15.19 h (2,2,4 VTCD). Generally speaking, the greater the WAC, the less damage the mushroom tissue sustains during drying and the better the drying quality. In large-scale factory production, the drying efficiency improves as the total drying time decreases. Therefore, we hope to obtain a drying process with high mushroom WAC and short total drying time to achieve a win–win situation between drying quality and drying efficiency. Figure 13 shows the VTCD processes sorted according to the ratio of WAC to total drying time, which can be referred to as the actual production of shiitake mushroom drying.

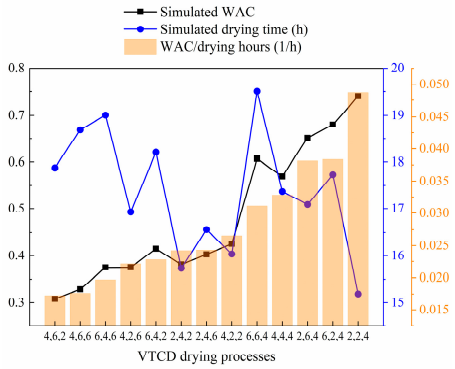


Figure 13. The effect of VTCD processes on WAC and total drying time.

4. Conclusions

Variable-temperature convective drying has less variation in shiitake mushroom temperature at the initial stage than with constant-temperature convective drying. Moreover, variable-temperature convective drying has a moderate shrinkage rate and less variation in evaporation rate. It can simultaneously achieve a high evaporation rate and a low evaporation rate gradient.

As for the drying load characteristics, variable-temperature convective drying demonstrates moderate total drying time (16.89 h) and better enthalpy stability, reducing the maximum drying load by 58.84% compared to 338.15 K constant-temperature convective drying.

The rehydration kinetics of shiitake mushrooms are modelled as a function of the drying time of each temperature zone in variable-temperature convective drying. All variable-temperature dried mushrooms exhibit superior rehydration performance better than those dried at a constant temperature of 338.15 K. The drying time at 318.15 K has the most significant impact on the rehydration kinetic parameters. The variable-temperature convective drying process with moderate drying time (4 h) at 328.15 K and short drying time (2 h) at low temperature (318.15 K) displays the best performance weighing the rehydration capacity and drying efficiency.

In conclusion, variable-temperature convective drying outperforms constant-temperature convective drying regarding dehydration characteristics, energy supply–demand matching, and rehydration performance. Nevertheless, further research is needed to explore other characteristic changes of shiitake mushrooms during variable-temperature convective drying processes, such as color, flavor compounds, and nutrients.

Supplementary Materials: The following supporting information can be downloaded at: https://www.mdpi.com/article/10.3390/foods13213356/s1.

Author Contributions: Conceptualization, L.Z.; Data curation, L.Z.; Formal analysis, L.Z.; Funding acquisition, X.Z.; Investigation, L.Z.; Methodology, L.Z.; Project administration, L.J. and X.Z.; Resources, L.J. and X.Z.; Supervision, L.J. and X.Z.; Validation, L.Z.; Writing—original draft, L.Z.; Writing—review and editing, L.Z., L.J., M.A. and S.L. All authors have read and agreed to the published version of the manuscript.

Funding: This research was supported by the Key Research and Development Program of Zhejiang Province (No. 2024C03117), National Natural Science Foundation of China (No. 52376017), and the Basic Research Funds for the Central University 'Innovative Team of Zhejiang University' under contract number (2022FZZX01-09).

Data Availability Statement: The original contributions presented in the study are included in the article, further inquiries can be directed to the corresponding authors.

Conflicts of Interest: The authors declare no conflicts of interest.

Appendix A. Formula Derivation of Mathematical Model Combining Drying and Rehydration

The mushroom's density is obtained by the density and volume fraction of each phase:

$$\rho_{m,0} = \rho_s x_{s,0} + \rho_{l,0} x_{l,0} + \rho_{ma,0}(1 - x_{s,0} - x_{l,0}) \quad \text{(A1)}$$

$$\rho_{m,d} = \frac{\rho_s x_{s,0}}{1 - SR} + \frac{\rho_l x_{l,0} MR}{1 - SR} + \rho_g \left(1 - \frac{x_{s,0}}{1 - SR} - \frac{x_{l,0} MR}{1 - SR}\right) \quad \text{(A2)}$$

where $\rho_{m,0}$ and $\rho_{m,d}$ represent the mushroom density before and after drying, respectively, kg/m^3; ρ_s, $\rho_{l,0}$, and $\rho_{ma,0}$ are the density of solid, liquid, and gas phases in shiitake mushroom before drying, respectively, kg/m^3; ρ_l and ρ_g are the density of liquid phase and gas phase in shiitake mushroom after drying, kg/m^3; $x_{s,0}$ and $x_{l,0}$ are the initial volume fraction of solid matrix and liquid water; MR is the moisture ratio; SR is the volume shrinkage ratio.

The mushroom mass ratio in the drying process is calculated by density ratio and volume shrinkage ratio.

$$\frac{m_0}{m_d} = \frac{\rho_{m,0} V_{m,0}}{\rho_{m,d} V_{m,d}} = \frac{\rho_{m,0}}{\rho_{m,d}} \times \frac{1}{1 - SR} \tag{A3}$$

The dry basis moisture contents are calculated from rehydration experimental results, and the rehydration kinetic parameters are fitted. Rehydration indices are derived.

$$X_{db,r} = \frac{m_r - m_{s,r}}{m_{s,r}} = \frac{m_r - DHC \times m_{s,d}}{DHC \times m_{s,d}} = \frac{m_r}{DHC \times m_{s,d}} - 1 \tag{A4}$$

$$X_{db,r} = X_{db,d} + \frac{t}{K_1 + K_2 \times t} \tag{A5}$$

$$X_{wb} = \frac{X_{db}}{1 + X_{db}} \tag{A6}$$

$$RR = \frac{m_r}{m_d} = \frac{m_{l,r} + m_{s,r}}{m_{l,d} + m_{s,d}} = \frac{m_{l,r} + DHC \times m_{s,d}}{m_{l,d} + m_{s,d}} = \frac{X_{db,r} + 1}{X_{db,d} + 1} DHC \tag{A7}$$

$$WAC = \frac{m_r(1 - s_r) - m_d(1 - s_d)}{m_0(1 - s_0) - m_d(1 - s_d)} = \frac{m_r X_{wb,r} - m_d X_{wb,d}}{m_0 X_{wb,0} - m_d X_{wb,d}} = \frac{RR X_{wb,r} - X_{wb,d}}{\frac{m_0}{m_d} X_{wb,0} - X_{wb,d}} \tag{A8}$$

where m_0, m_d, and m_r are the shiitake mushroom mass before drying, after drying, and after rehydration, respectively, kg; $V_{m,0}$ and $V_{m,d}$ represent the shiitake mushroom volumes before and after drying, m^3; DHC is the dry matter holding capacity during rehydration; RR is the rehydration ratio; $m_{l,r}$ and $m_{s,r}$ are the mass of liquid water and solid matrix in mushroom after rehydration, kg; $m_{l,d}$ and $m_{s,d}$ are the mass of liquid water and solid matrix in mushroom after drying, kg; $X_{db,r}$ and $X_{db,d}$ are the dry basis moisture content after and before rehydration; WAC is the water absorption capacity during rehydration; s_0, s_d, and s_r are the dry matter content of initial, dried, and rehydrated mushrooms, respectively; $X_{wb,0}$, $X_{wb,d}$, and $X_{wb,r}$ represent the wet-basis moisture content of initial, dried, and rehydrated mushrooms, respectively.

Appendix B. Temperature and Evaporation Rate Distribution of Shiitake Mushrooms in VTCD and CTCD Processes

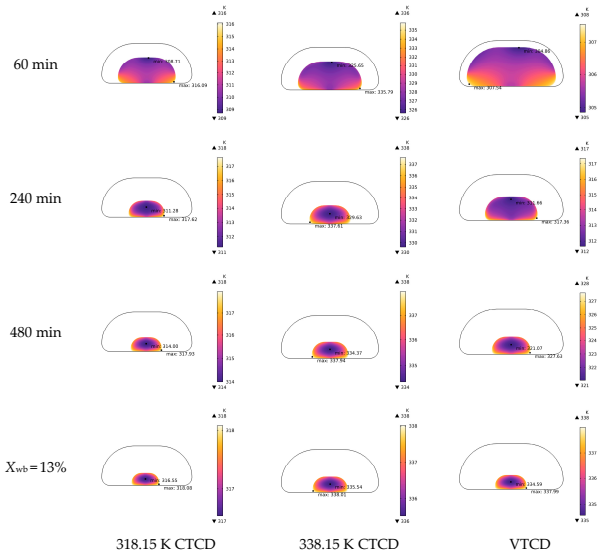


Figure A1. Temperature distribution of shiitake mushrooms in VTCD and CTCD processes.

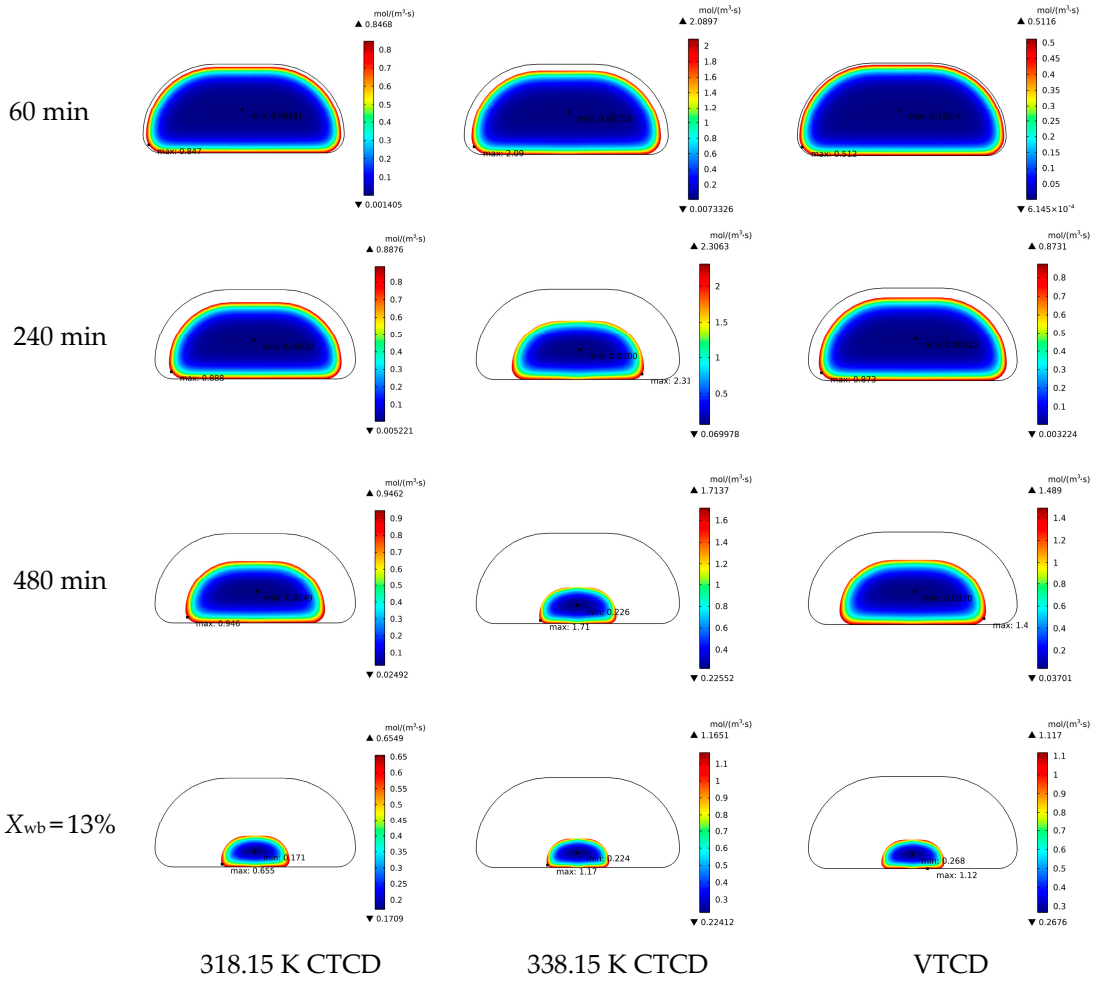


Figure A2. Evaporation rate distribution of shiitake mushrooms in VTCD and CTCD processes.

References

1. Jiang, T.; Wang, Q.; Xu, S.; Jahangir, M.M.; Ying, T. Structure and Composition Changes in the Cell Wall in Relation to Texture of Shiitake Mushrooms (*Lentinula edodes*) Stored in Modified Atmosphere Packaging. *J. Sci. Food Agric.* **2010**, *90*, 742–749. [CrossRef] [PubMed]
2. Lu, W.; Wu, D.; Wang, L.; Song, G.; Chi, R.; Ma, J.; Li, Z.; Wang, L.; Sun, W. Insoluble Dietary Fibers from *Lentinus edodes* Stipes Improve the Gel Properties of Pork Myofibrillar Protein: A Water Distribution, Microstructure and Intermolecular Interactions Study. *Food Chem.* **2023**, *411*, 135386. [CrossRef]
3. Cheng, S.; Li, R.; Yang, H.; Wang, S.; Tan, M. Water Status and Distribution in Shiitake Mushroom and the Effects of Drying on Water Dynamics Assessed by Lf-Nmr and Mri. *Dry. Technol.* **2020**, *38*, 1001–1010. [CrossRef]
4. Subramaniam, S.; Jiao, S.; Zhang, Z.; Jing, P. Impact of Post-Harvest Processing or Thermal Dehydration on Physiochemical, Nutritional and Sensory Quality of Shiitake Mushrooms. *Compr. Rev. Food Sci. Food Saf.* **2021**, *20*, 2560–2595. [CrossRef] [PubMed]
5. Hiraide, M.; Miyazaki, Y.; Shibata, Y. The Smell and Odorous Components of Dried Shiitake Mushroom, Lentinula Edodes I: Relationship between Sensory Evaluations and Amounts of Odorous Components. *J. Wood Sci.* **2004**, *50*, 358–364. [CrossRef]
6. Jasinghe, V.J.; Perera, C.O. Ultraviolet Irradiation: The Generator of Vitamin D2 in Edible Mushrooms. *Food Chem.* **2006**, *95*, 638–643. [CrossRef]
7. Abdelshafy, A.M.; Luo, Z.; Belwal, T.; Ban, Z.; Li, L. A Comprehensive Review on Preservation of Shiitake Mushroom (*Lentinus edodes*): Techniques, Research Advances and Influence on Quality Traits. *Food Rev. Int.* **2021**, *39*, 2742–2775. [CrossRef]
8. Adnouni, M.; Jiang, L.; Zhang, X.J.; Zhang, L.Z.; Pathare, P.B.; Roskilly, A.P. Computational Modelling for Decarbonised Drying of Agricultural Products: Sustainable Processes, Energy Efficiency, and Quality Improvement. *J. Food Eng.* **2023**, *338*, 111247. [CrossRef]
9. Seo, J.-S.; Gang, S.-G.; Choe, B.-M. Drying Characteristics and Content Change of Major Components of Shiitake Mushroom (*Lentinus edodes*) 2. Changes in Major Components of Shiitake Mushroom by Drying Temperature. *Korean J. Food Preserv.* **1997**, *4*, 279–286.
10. Timm, T.G.; Pasko, R.Z.; Campos, C.S.d.G.; Helm, C.V.; Tavares, L.B.B. Drying Process of Lentinula Edodes: Influence of Temperature on B-Glucan Content and Adjustment of Mathematical Models. *Ciência E Agrotecnologia* **2020**, *43*, e025719. [CrossRef]

11. Li, W.; Li, R.; Chen, W.; Feng, J.; Wu, D.; Zhang, Z.; Zhang, J.; Yang, Y. The Anabolism of Sulphur Aroma Volatiles Responds to Enzymatic and Non-Enzymatic Reactions During the Drying Process of Shiitake Mushrooms. *Food Chem.* **2022**, *371*, 131123. [CrossRef] [PubMed]
12. Wang, H.; Che, G.; Wan, L.; Tang, H. Effects of Drying Approaches Combined with Variable Temperature and Tempering on the Physicochemical Quality of Rice. *Dry. Technol.* **2022**, *41*, 1199–1213. [CrossRef]
13. Bin, Y.; Xu-kun, Z.; Xiang-dong, W.; Jia-fu, Z. Developments of Variable Temperature Drying Technology for Agricultural Products at Home and Abroad. *Food Sci. Technol.* **2015**, *40*, 94–98. [CrossRef]
14. Chasiotis, V.; Nikas, K.-S.; Filios, A. Modeling and Optimization of Non-Isothermal Convective Drying Process of *Lavandula* × *allardii*. *Inf. Process. Agric.* **2022**, *11*, 1–13. [CrossRef]
15. Zhang, L.; Yu, X.; Arun, S.M.; Zhou, C. Effect of Freeze-Thaw Pretreatment Combined with Variable Temperature on Infrared and Convection Drying of Lotus Root. *LWT* **2022**, *154*, 112804. [CrossRef]
16. Ayadi, M.; Mabrouk, S.B.; Zouari, I.; Bellagi, A. Kinetic Study of the Convective Drying of Spearmint. *J. Saudi Soc. Agric. Sci.* **2014**, *13*, 1–7. [CrossRef]
17. Zhang, L.Z.; Jiang, L.; Xu, Z.C.; Zhang, X.J.; Fan, Y.B.; Adnouni, M.; Zhang, C.B. Optimization of a Variable-Temperature Heat Pump Drying Process of Shiitake Mushrooms Using Response Surface Methodology. *Renew. Energy* **2022**, *198*, 1267–1278. [CrossRef]
18. Men, K.; Huang, D.; Qin, Y.; Zhang, X.; Tang, X.; Gong, G.; Li, L. Optimization of Variable-Temperature Drying of Camellia Oleifera Seeds. *Proc. Inst. Mech. Eng. Part E J. Process Mech. Eng.* **2022**, *237*, 220–228. [CrossRef]
19. Zeng, S.; Du, Z.; Lv, W.; Li, D.; Su, D.; Lv, H. Experimental Study on the Hygrothermal Dynamics of Peanut (Arachis Hypogaea Linn.) in the Process of Superposition and Variable Temperature Drying. *Dry. Technol.* **2022**, *40*, 1463–1477. [CrossRef]
20. Babu, A.K.; Kumaresan, G.; Raj, V.A.A.; Velraj, R. Review of Leaf Drying: Mechanism and Influencing Parameters, Drying Methods, Nutrient Preservation, and Mathematical Models. *Renew. Sustain. Energy Rev.* **2018**, *90*, 536–556. [CrossRef]
21. Taghinezhad, E.; Kaveh, M.; Jahanbakhshi, A.; Golpour, I. Use of Artificial Intelligence for the Estimation of Effective Moisture Diffusivity, Specific Energy Consumption, Color and Shrinkage in Quince Drying. *J. Food Process Eng.* **2020**, *43*, e13358. [CrossRef]
22. Gulati, T.; Datta, A.K. Mechanistic Understanding of Case-Hardening and Texture Development During Drying of Food Materials. *J. Food Eng.* **2015**, *166*, 119–138. [CrossRef]
23. Ahn, S.P.; Kim, S.H.; Park, Y.G.; Ha, M.Y. Experimental Study on Drying Time and Energy Consumption of a Vented Dryer. *J. Mech. Sci. Technol.* **2019**, *33*, 2471–2480. [CrossRef]
24. Li, B.; Zeng, Z.; Zhang, X.; Zhang, Y. Study on the Variable-Temperature Drying Process of Corn Drying in an Industrial Corn-Drying System Equipped with a Self-Adaptive Control Heat Exchanger. *Appl. Sci.* **2021**, *11*, 2772. [CrossRef]
25. Contreras, C.; Martín-Esparza, M.E.; Martínez-Navarrete, N. Influence of Drying Method on the Rehydration Properties of Apricot and Apple. *J. Food Process Eng.* **2012**, *35*, 178–190. [CrossRef]
26. Aravindakshan, S.; Nguyen, T.H.A.; Kyomugasho, C.; Buvé, C.; Dewettinck, K.; Van Loey, A.; Hendrickx, M.E. The Impact of Drying and Rehydration on the Structural Properties and Quality Attributes of Pre-Cooked Dried Beans. *Foods* **2021**, *10*, 1665. [CrossRef] [PubMed]
27. García-Segovia, P.; Andrés-Bello, A.; Martínez-Monzó, J. Rehydration of Air-Dried Shiitake Mushroom (*Lentinus edodes*) Caps: Comparison of Conventional and Vacuum Water Immersion Processes. *LWT—Food Sci. Technol.* **2011**, *44*, 480–488. [CrossRef]
28. Qiu, Y.; Bi, J.; Jin, X.; Hu, L.; Lyu, J.; Wu, X. An Understanding of the Changes in Water Holding Capacity of Rehydrated Shiitake Mushroom (Lentinula Edodes) from Cell Wall, Cell Membrane and Protein. *Food Chem.* **2021**, *351*, 129230. [CrossRef]
29. Subramaniam, S.; Wen, X.-Y.; Zhang, Z.-T.; Jing, P. Changes in the Morphometric, Textural, and Aromatic Characteristics of Shiitake Mushrooms During Combined Humid-Convective Drying. *Dry. Technol.* **2021**, *39*, 2206–2217. [CrossRef]
30. Zhang, J.; Yagoub, A.E.A.; Sun, Y.; Arun, M.S.; Ma, H.; Zhou, C. Role of Thermal and Non-Thermal Drying Techniques on Drying Kinetics and the Physicochemical Properties of Shiitake Mushroom. *J. Sci. Food Agric.* **2022**, *102*, 214–222. [CrossRef]
31. Xu, L.; Fang, X.; Wu, W.; Chen, H.; Mu, H.; Gao, H. Effects of High-Temperature Pre-Drying on the Quality of Air-Dried Shiitake Mushrooms (*Lentinula edodes*). *Food Chem.* **2019**, *285*, 406–413. [CrossRef] [PubMed]
32. Wang, H.; Zhang, M.; Mujumdar, A.S. Comparison of Three New Drying Methods for Drying Characteristics and Quality of Shiitake Mushroom (*Lentinus edodes*). *Dry. Technol.* **2014**, *32*, 1791–1802. [CrossRef]
33. Hu, L.; Bi, J.; Jin, X.; Qiu, Y.; Sman, R. Study on the Rehydration Quality Improvement of Shiitake Mushroom by Combined Drying Methods. *Foods* **2021**, *10*, 769. [CrossRef]
34. Dai, J.-A.; fa Diao, Y. Numerical Analysis of Transient Coupled Heat and Moisture Transfer in Textile Drying with Porous Relative Impact Jet. *Appl. Therm. Eng.* **2022**, *212*, 118613. [CrossRef]
35. Ousegui, A.; Moresoli, C.; Dostie, M.; Marcos, B. Porous Multiphase Approach for Baking Process—Explicit Formulation of Evaporation Rate. *J. Food Eng.* **2010**, *100*, 535–544. [CrossRef]
36. Ni, H.; Datta, A.K.; Torrance, K.E. Moisture Transport in Intensive Microwave Heating of Biomaterials: A Multiphase Porous Media Model. *Int. J. Heat Mass Transf.* **1999**, *42*, 1501–1512. [CrossRef]
37. Zhu, Y.; Wang, P.; Sun, D.; Qu, Z.; Yu, B. Multiphase Porous Media Model with Thermo-Hydro and Mechanical Bidirectional Coupling for Food Convective Drying. *Int. J. Heat Mass Transf.* **2021**, *175*, 121356. [CrossRef]
38. Datta, A.K. Porous Media Approaches to Studying Simultaneous Heat and Mass Transfer in Food Processes. Ii: Property Data and Representative Results. *J. Food Eng.* **2007**, *80*, 96–110. [CrossRef]

39. Millington, R.J.; Quirk, J.P. Permeability of Porous Solids. *Trans. Faraday Soc.* **1961**, *57*, 1200–1207. [CrossRef]
40. Datta, A.K. Porous Media Approaches to Studying Simultaneous Heat and Mass Transfer in Food Processes. I: Problem Formulations. *J. Food Eng.* **2007**, *80*, 80–95. [CrossRef]
41. Bennamoun, L.; Belhamri, A. Mathematical Description of Heat and Mass Transfer During Deep Bed Drying: Effect of Product Shrinkage on Bed Porosity. *Appl. Therm. Eng.* **2008**, *28*, 2236–2244. [CrossRef]
42. Castro, A.M.; Mayorga, E.Y.; Moreno, F.L. Mathematical Modelling of Convective Drying of Fruits: A Review. *J. Food Eng.* **2018**, *223*, 152–167. [CrossRef]
43. Ozturk, O.K.; Singh Takhar, P. Selected Physical and Viscoelastic Properties of Strawberries as a Function of Heated-Air Drying Conditions. *Dry. Technol.* **2019**, *37*, 1833–1843. [CrossRef]
44. Ozturk, O.K.; Takhar, P.S. Physical and Viscoelastic Properties of Carrots During Drying. *J. Texture Stud.* **2020**, *51*, 532–541. [CrossRef]
45. Rojas, M.L.; Augusto, P.E.D. Ethanol Pre-Treatment Improves Vegetable Drying and Rehydration: Kinetics, Mechanisms and Impact on Viscoelastic Properties. *J. Food Eng.* **2018**, *233*, 17–27. [CrossRef]
46. Hu, L.; Bi, J.; Jin, X.; van der Sman, R. Impact of Physical Changes in Mushroom on Variation in Moisture Sorption. *J. Food Eng.* **2023**, *351*, 111506. [CrossRef]
47. Halder, A.; Dhall, A.; Datta, A.K. An Improved, Easily Implementable, Porous Media Based Model for Deep-Fat Frying: Part I: Model Development and Input Parameters. *Food Bioprod. Process.* **2007**, *85*, 209–219. [CrossRef]
48. Zhang, J.; Datta, A.K.; Rakesh, V. Investigation of Non-Equilibrium in Water Evaporation. In Proceedings of the 3rd Inter-American Drying Conference, Montreal, QC, Canada, 21–23 August 2005.
49. Zhao, J.-H.; Ding, Y.; Nie, Y.; Xiao, H.-W.; Zhang, Y.; Zhu, Z.; Tang, X.-M. Glass Transition and State Diagram for Freeze-Dried *Lentinus edodes* Mushroom. *Thermochim. Acta* **2016**, *637*, 82–89. [CrossRef]
50. Oikonomopoulou, V.P.; Krokida, M.K. Structural Properties of Dried Potatoes, Mushrooms, and Strawberries as a Function of Freeze-Drying Pressure. *Dry. Technol.* **2012**, *30*, 351–361. [CrossRef]
51. Tansakul, A.; Lumyong, R. Thermal Properties of Straw Mushroom. *J. Food Eng.* **2008**, *87*, 91–98. [CrossRef]
52. Mantecón, J.G.; Neto, M.M. Simplified Cfd Model of Coolant Channels Typical of a Plate-Type Fuel Element: An Exhaustive Verification of the Simulations. *Braz. J. Radiat. Sci.* **2019**, *7* (Suppl. S2B), 1–16. [CrossRef]
53. Peleg, M. An Empirical Model for the Description of Moisture Sorption Curves. *J. Food Sci.* **1988**, *53*, 1216–1217. [CrossRef]
54. Kaleta, A.; Górnicki, K.; Choinska, A.; Kosiorek, K.; Czyzewska, A. Modelling of Rehydration Kinetics of Dried Carrots Using the Peleg Model. *Agri-For. Eng* **2017**, *69*, 13–21. [CrossRef]
55. Okpala, L.C.; Ekechi, C.A. Rehydration Characteristics of Dehydrated West African Pepper (*Piper guineense*) Leaves. *Food Sci. Nutr.* **2014**, *2*, 664–668. [CrossRef]
56. Salimi Hizaji, A.; Maghsoudlou, Y.; Jafari, S.M. Application of Peleg Model to Study Effect of Water Temperature and Storage Time on Rehydration Kinetics of Air Dried Potato Cubes. *Lat. Am. Appl. Res.* **2010**, *40*, 131–136.
57. Hernando, I.; Sanjuán, N.; Pérez-Munuera, I.; Mulet, A. Rehydration of Freeze-Dried and Convective Dried Boletus Edulis Mushrooms: Effect on Some Quality Parameters. *J. Food Sci.* **2008**, *73*, E356–E362. [CrossRef]
58. García-Pascual, P.; Sanjuán, N.; Melis, R.; Mulet, A. *Morchella esculenta* (Morel) Rehydration Process Modelling. *J. Food Eng.* **2006**, *72*, 346–353. [CrossRef]
59. Okos, M.R.; Narsimhan, G.; Singh, R.K.; Weitnauer, A.C.; Heldman, D.; Lund, D. Food Dehydration. In *Handbook of Food Engineering*; CRC Press: Boca Raton, FL, USA, 2019; pp. 437–562. [CrossRef]
60. Lewicki, P.P. Some Remarks on Rehydration of Dried Foods. *J. Food Eng.* **1998**, *36*, 81–87. [CrossRef]
61. Wang, X.; Feng, Y.; Zhou, C.; Sun, Y.; Wu, B.; Yagoub, A.E.A.; Aboagarib, E.A.A. Effect of Vacuum and Ethanol Pretreatment on Infrared-Hot Air Drying of Scallion (*Allium fistulosum*). *Food Chem.* **2019**, *295*, 432–440. [CrossRef]
62. Lewicki, P.P. Effect of Pre-Drying Treatment, Drying and Rehydration on Plant Tissue Properties: A Review. *Int. J. Food Prop.* **1998**, *1*, 1–22. [CrossRef]
63. Moreira, R.; Chenlo, F.; Chaguri, L.; Fernandes, C. Water Absorption, Texture, and Color Kinetics of Air-Dried Chestnuts During Rehydration. *J. Food Eng.* **2008**, *86*, 584–594. [CrossRef]
64. Guo, X.H.; Xia, C.Y.; Tan, Y.R.; Chen, L.; Ming, J. Mathematical Modeling and Effect of Various Hot-Air Drying on Mushroom (*Lentinus edodes*). *J. Integr. Agric.* **2014**, *13*, 207–216. [CrossRef]
65. Goncalves, M.d.P.; Tojo, S.; Nazari, S.A.M.; Silveira Junior, V. Alternative Freezing: Effects on Rehydration Properties of Freeze-Dried Daikon (*Raphanus sativus* L.). *J. Food Process Eng.* **2021**, *44*, e13686. [CrossRef]
66. Maskan, M. Effect of Processing on Hydration Kinetics of Three Wheat Products of the Same Variety. *J. Food Eng.* **2002**, *52*, 337–341. [CrossRef]
67. Planinić, M.; Velić, D.; Tomas, S.; Bilić, M.; Bucić, A. Modelling of Drying and Rehydration of Carrots Using Peleg's Model. *Eur. Food Res. Technol.* **2005**, *221*, 446–451. [CrossRef]

Disclaimer/Publisher's Note: The statements, opinions and data contained in all publications are solely those of the individual author(s) and contributor(s) and not of MDPI and/or the editor(s). MDPI and/or the editor(s) disclaim responsibility for any injury to people or property resulting from any ideas, methods, instructions or products referred to in the content.